Spectroscopy of Hydrothermal Reactions. 14. Kinetics of the pH-Sensitive Aminoguanidine−Semicarbazide−Cyanate Reaction Network

A. J. Belsky and T. B. Brill*

Department of Chemistry and Biochemistry, University of Delaware, Newark, Delaware 19711

Received: June 9, 1999; In Final Form: August 6, 1999

Infrared spectroscopy in conjunction with an optically accessed flow reactor enable real-time concentration measurements to be made on species involved in hydrothermal reactions. The kinetics of the reaction of the aqueous cyanate ion, OCN^-, at 110−160 °C and 275 bar were determined at pH = 3.94−10.5. These kinetics are useful because OCN^- is frequently the precursor to the NH_3 and CO_2 products seen during the hydrothermolysis of organic amines. Three rate constants were needed to model the cyanate reaction. These rates were then used to model the hydrothermolysis kinetics of the progressively more complex reactions of the isoelectronic cations of semicarbazide (T = 140−170 °C) and aminoguanidine (T = 190−260 °C) in neutral and acidic solutions. Six internally consistent rate constants were obtained in order to specify the reaction network.

Introduction

The cyanate ion, OCN^-, is a common, later-stage product of hydrothermal reactions of organic amines[1−5] and is one source of the relatively stable and inert end products CO_2 and NH_3. Because the $-NH_2$ and $-CO_2H$ groups[6−8] are arguably penultimate functionalities in aqueous organic chemistry, the kinetics of conversion of OCN^- as a function of the pH is an essential component in models of the reaction of simple organic amines. To date, however, these kinetic data are only known for the normal liquid range of H_2O[2,9−12] except in the case of NH_4OCN, which forms during the hydrothermolysis of urea solutions.[1,4]

The kinetics of conversion of aqueous NaOCN to CO_2 and NH_3 are described here at T = 110−160 °C and P = 275 bar in the initial pH range at 22 °C of 3.94−10.5. Concentration vs time profiles were constructed from the absorbances of IR-active species measured with a flow reactor. Rate constants for three regimes were required to model these data. These rate constants permit the kinetics to be determined for more complex molecules that eventually form the OCN^- ion during the reaction. The isoelectronic semicarbazide (SCA^+) and aminoguanidinium

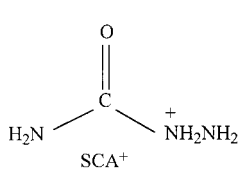

SCA^+

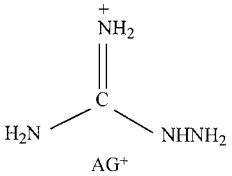

AG^+

(AG^+) cations are examples of such molecules. Each was characterized as a function of the pH with the aid of the OCN^- data. The method here of initially determining the product network kinetics and then working backward to model the kinetics of the more complex reactants is a systematic means to test the consistency of progressively more complex and competitive reaction networks.[5,13]

Experimental Section

Aminoguanidinium nitrate ($H_2NNHC(=NH)NH_2 \cdot HNO_3$), semicarbazide hydrochloride [$H_2NC(O)NHNH_2 \cdot HCl$], hydrazine, and sodium cyanate (NaOCN) were obtained from the Aldrich Chemical Co. Each had a stated purity of >96% and was used as received. Semicarbazide hydrochloride was converted to the nitrate salt by adding a stoichiometric amount of $AgNO_3$ in H_2O solution. These nitrate salts are referred to herein as AGN and SCAN for the aminoguanidine (AG^+) and semicarbazide (SCA^+) cations, respectively. The aqueous solutions for the kinetics studies were then made from Milli-Q water, which had been sparged with Ar to remove atmospheric gases. Concentrations were 1.0 *m* (*m* = molal) for AGN and 0.25 *m* for SCAN and NaOCN. AGN was investigated at the higher concentration in the hope of observing the IR absorption of OCN^- more clearly. The initial pH was determined using an Orion 330 pH meter with an Ag/AgCl perpHect electrode calibrated at multiple points by the use of standard buffer solutions. HNO_3 or NaOH solutions were used to adjust the pH into the other ranges used in this study. The NO_3^- ion is a spectator under the conditions of these experiments.[1,4]

The laboratory-scale flow reactor−spectroscopy cell[1,4] was constructed from grade 2 titanium into which two 0° sapphire windows were seated. Gold-foil washers were compressed at each interface to form the seals. The solution flowed in a flat duct that was created between the two sapphire windows by a slot cut into the gold foil spacer. The path length (the thickness of the flat duct) was (30−35) ± 1 μm as determined by the absorbance of a known concentration of aqueous CO_2 flowing through the cell.[14] The temperature (±1 °C) was controlled by using proportional integral−differential controllers, the pressure (±1 bar) was controlled by a pneumatic bleed-and-lock system, and the constant flow rate was maintained with an Isco syringe

* To whom correspondence should be sent. E-mail: brill@udel.edu.

10.1021/jp991878j CCC: $18.00
Published on Web 09/10/1999

TABLE 1: p*K* Values of the Salts Used

	p*K* value			
temp, °C	NaOCN	SCAN	AGN	$[N_2H_5]NO_3$
25	5.08	10.31	3.98	8.12
30	5.10	10.19	3.82	8.41

pump. A single liquid phase existed at all times as indicated by the absence of IR modes for water vapor and the condition of the spectral baseline.

A few studies were conducted with a cell constructed from 316 stainless steel (SS). This alloy is risky to use in these studies because of the potential for corrosion by HNO_3. An interesting result was obtained for AGN where there was evidence that the $[N_2H_5]NO_3$ decomposition product converted to N_2O (and other species) in the 316 SS cell but not in the Ti cell. All of the kinetic measurements were therefore made with the Ti cell.

The kinetics were modeled by assuming plug−flow conditions. This necessitated the use of flow rates that resulted in residence times of 4−45 s and degrees of conversion of ≤40%. The true residence time at each temperature was obtained by dividing the internal volume of the cell (entrance tube and flat duct), which was 0.0819 cm^3, by the expression (volume flow rate)($\rho_{25°C}/\rho_T$). The density correction is needed because the density of water depends on the temperature (e.g., $\rho_{100°C} = 0.97$ g/cm^3, $\rho_{260°C} = 0.81$ g/cm^3 at a constant pressure of 275 bar).

A Nicolet 560 Magna FTIR spectrometer equipped with a liquid-N_2-cooled MCT-A detector was used for real-time IR spectral measurements in the flow reactor. Thirty-two spectra were summed at 4 cm^{-1} resolution (∼10 s total collection time) at each flow rate and temperature. The IR spectra were normalized with the background spectra of pure water recorded at the same pressure and temperature. The areas of the strongly IR-active OCN^- asymmetric stretch (2167 cm^{-1}), the CO_2 asymmetric stretch (2343 cm^{-1}), and the carbonyl stretch of SCA^+ (1716 cm^{-1}) were obtained by fitting the line shape with a four-parameter Voigt function in Matlab. The lower frequency wing of the SCA^+ mode was modeled as the mirror image of the higher frequency wing. A broad absorbance at 2400 cm^{-1} was observed in AGN and several SCAN spectra and was also previously observed in the IR spectrum of aqueous guanidinium nitrate under hydrothermal conditions.[4] This absorption is believed to be an overtone or a combination band of NO_3^- activated by association with AG^+ and SCA^+. It was fitted with a Gaussian function in Matlab. Three data sets were recorded for each compound. The average of the rates (k_{ave}) and the standard deviation (σ_k) were obtained from least squares regression and provide the value and error of each rate constant and the Arrhenius parameters. Two regression methods were used to fit the Arrhenius parameters:[15,16] an Arrhenius-weighted least-squares regression was used for k_1-k_5 (higher temperature rate data weighted more than lower temperature data, $w = (k^2/\sigma_k^2)$; and a linear regression was used for k_6 (all data weighted equally, $w = 1$). The expression ($\ln k_{ave} \pm \sigma_k/k_{ave}$) was used when converting the errors into log space.[15,16]

The ionization equilibrium constants for the acids and bases in this study were used extensively in the charge balance equations. The p*K* values of CO_2,[17] NH_3,[18] NaOH,[19] and HNO_3[19] were taken from the literature. The p*K* values for AG^+, SCA^+, $N_2H_5^+$, and OCN^- were obtained from the temperature dependence of the pH of aqueous solutions using the pH meter described above. Table 1 gives the p*K* values for these salts, which were then used to determine the p*K* values at the higher temperature reactions using the iso-Coulombic method.[20] The iso-Coulombic method enables the equilibrium constant to be

SCHEME 1

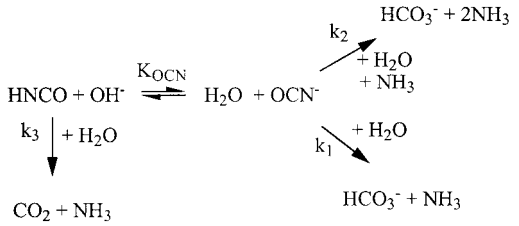

extrapolated linearly from one temperature range to another. As an example, the iso-Coulombic form of the equilibrium constant for HNO_3 is shown in eq 1, where $K_{HNO_3} = K_W/K_a$. The temperature dependence of the ion product of H_2O,

$$NO_3^- + H_2O \overset{K_{HNO_3}}{\rightleftharpoons} HNO_3 + OH^- \quad (1)$$

K_W, is available over a wide temperature range.[21] The iso-Coulombic expressions for CO_2, NH_3, and N_2H_4 are given by

$$CO_2 + OH^- \overset{K_1}{\rightleftharpoons} HCO_3^- \quad (2)$$

$$HCO_3^- + OH^- \overset{K_2}{\rightleftharpoons} CO_3^{2-} + H_2O \quad (3)$$

$$NH_3 + H_3O^+ \overset{K_N}{\rightleftharpoons} NH_4^+ + H_2O \quad (4)$$

$$N_2H_5^+ + H_2O \overset{K_{N_2H_4}}{\rightleftharpoons} N_2H_4 + H_3O^+ \quad (5)$$

Other such relations are defined in the text as they are used.

Kinetics of OCN^-. Several studies report the hydrolysis kinetics of OCN^- in acid, neutral, and basic solutions over the 4−100 °C range.[2,9−12] Mostly classical analytical methods were used, and the rates were occasionally based on only two reaction times. The errors in the measurements are generally not known. Reactions 6 (acidic), 7 (neutral), and 8 (basic),

$$HNCO + H_3O^+ \rightarrow CO_2 + NH_4^+ \quad (6)$$

$$HNCO + H_2O \rightarrow CO_2 + NH_3 \quad (7)$$

$$OCN^- + 2H_2O \rightarrow HCO_3^- + NH_3 \quad (8)$$

are, however, generally accepted,[9,11,12] and they are simple variations of essentially the same process. Several details of reactions 6−8 have been suggested, including evidence that the HNCO isomer is favored over HOCN as the temperature is raised,[22] a carbamic acid intermediate forms in reaction 6,[10,23] and HCO_3^-,[11] CO_2,[2−9] and NH_3[24] are catalysts for reaction 8. The rate constants for reactions 6−8 were previously determined separately in each case and not modeled as one competitive scheme. Hence, the effect of a variable value of the pH on the hydrolysis rate was not previously known.

The natural pH of aqueous NaOCN at 25 °C is 10.5. Beginning with the premise that reactions 6−8 describe the hydrothermolysis mechanism of cyanate species over a wide pH range, the reactions in Scheme 1 were used to model the concentration−time profiles of OCN^- for the hydrothermal regime (110−160 °C at 275 bar) as a function of pH. Figure 1 contains spectra showing the decreased intensity of the OCN asymmetric stretching mode in 0.25 *m* NaOCN at 160 °C for several flow reactor residence times. The amount of HNCO in NaOCN at 160 °C is <0.2% based on the iso-Coulombic

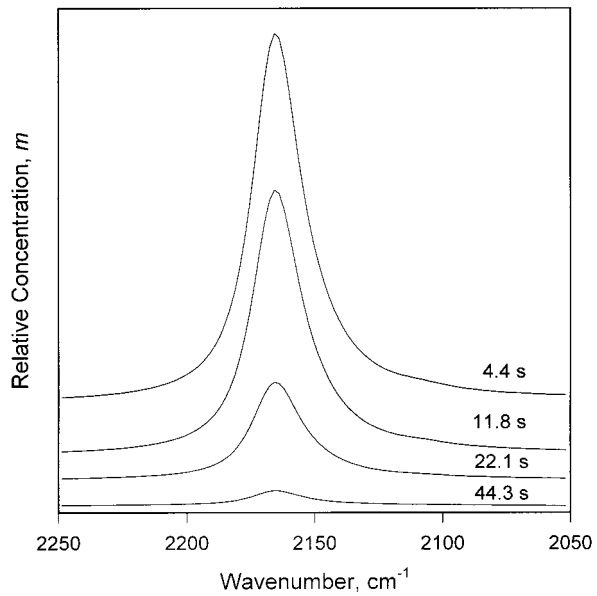

Figure 1. OCN^- stretching frequency of 0.25 *m* NaOCN with the residence times shown at 160 °C and 275 bar.

extrapolation of K_{OCN} from 25 °C. The spectra in Figure 1 are therefore reflective of the hydrated OCN^- ion. Similar kinetics data were gathered for NaOCN solutions with initial pH values of 10.35, 6.25, 5.70, and 3.94 by adding HNO_3. Of course, more HNCO forms as the pH is lowered.

The model of the kinetics of conversion of OCN^- at pH = 10.35 and 10.5 did not require that $[OH^-]$ be specified as a function of time, but the lower pH ranges require this information. The charge balance of

$$[H^+] + [NH_4^+] + [Na^+] = [OH^-] + [HCO_3^-] + 2[CO_3^{2-}] + [OCN^-] \quad (9)$$

is given in the parametrized version by

$$\frac{K_W}{[OH^-]} + \frac{[N_T]K_N\dfrac{K_W}{[OH^-]}}{K_W + K_N\dfrac{K_W}{[OH^-]}} + \frac{[Na_T^+]K_{Na^+}\dfrac{K_W}{[OH^-]}}{K_W + K_{Na^+}\dfrac{K_W}{[OH^-]}} = [OH^-] + \frac{[CO_{2T}]\dfrac{K_W}{[OH^-]}}{K_2 + \dfrac{K_W}{[OH^-]}} + 2\left([CO_{2T}] - \frac{[CO_{2T}]\dfrac{K_W}{[OH^-]}}{K_2 + \dfrac{K_W}{[OH^-]}}\right) + \frac{[OCN_T^-]K_{OCN^-}}{K_{OCN^-} + \dfrac{K_W}{[OH^-]}} \quad (10)$$

The equilibrium constants and species concentrations can be specified uniquely at each residence time and temperature so that $[OH^-]$ is known throughout. $N_T = [NH_3] + [NH_4^+]$; $[CO_{2T}] = [CO_2] + [HCO_3^-] + [CO_3^{2-}]$; $[OCN_T^-] = [OCN^-] + [HNCO]$; and $[Na_T] = [Na^+] + [NaOH]$. CO_2 was not observed under these basic solutions but was needed for the models at the lower pH values, which are described below.

By use of the spectral data and concentration relations at each residence time and temperature, the rate eq 11 was solved by optimizing the values of k_1 and k_2:

$$\frac{-d[OCN^-]}{dt} = k_1[OCN^-] + k_2[OCN^-][NH_3] \quad (11)$$

Rate constant k_1 was obtained by fitting the lower temperature data and also the initial stage of conversion in the higher temperature data. By use of this value of k_1, k_2 was then determined by fitting the later stages of conversion in the higher temperature data. The resulting values of k_1 and k_2 are listed in Table 2, and Figure 2 compares the experimental and calculated concentrations. Owing to the larger value of K_W, the initial pH at 140 °C is about 9.0. The pH decreased slightly as the reaction progressed because CO_2 is formed, but then the solution became buffered by the $NH_3-CO_2-H_2O$ equilibrium. As is apparent from eq 11, k_1 is the pseudo-first-order rate constant of hydrolysis of OCN^-. The value has been reported previously at 22 [2] and 70−94 °C.[3] Comparisons of the rate constants obtained for the hydrothermal regime with those previously reported for the normal liquid range of H_2O will be given later in this article. The rate constant k_2 captures the apparent acceleration of the rate with time, which suggests that an autocatalytic process is in effect. NH_3 is shown in Scheme 1 as the catalyst[24] rather than HCO_3^- or CO_3^{2-}, which were suggested elsewhere,[9,11,12] because we observed that the addition of Na_2CO_3 did not affect the reaction rate in the hydrothermal regime. The apparent autocatalytic effect of NH_3 might be caused by the formation of NH_4^+, which can in turn form a contact ion pair through hydrogen bonding with the cyanate O or N atom.[25] Such an association may facilitate the formation of a carbamate ($NH_2CO_2^-$) intermediate[2,10,23] in reaction 8.

The addition of HNO_3 reduced the pH of the NaOCN solution. A very slight reduction of the pH from an initial value of 10.5 to 10.35 had no effect on the reaction rate. The rate increased when the pH was reduced further to 6.25 and 5.7 as illustrated in Figure 3. As shown in Scheme 1 the initial $[OCN^-]$ decreases with a decrease of the pH because some of the OCN^- forms HNCO, which reacts before the experiment can commence. Equation 12

$$[H^+] + [NH_4^+] + [Na^+] = [OH^-] + [HCO_3^-] + [NO_3^-] + [OCN^-] \quad (12)$$

gives the charge balance, and eq 13

$$[H^+] + \frac{[N_T]K_N[H^+]}{K_W + K_N[H^+]} + \frac{[Na_T^+]K_{Na^+}[H^+]}{K_W + K_{Na^+}[H^+]} = \frac{K_W}{[H^+]} + \frac{[CO_{2T}]K_1}{K_1 + [H^+]} + \frac{[HNO_{3T}]K_{HNO_3}}{K_{HNO_3} + [H^+]} + \frac{[OCN_T^-]K_{OCN^-}}{K_{OCN^-} + [H^+]} \quad (13)$$

gives the running $[H^+]$ expression based on parametrization of eq 12 with equilibrium constants and concentrations. $[HNO_{3T}] = [HNO_3] + [NO_3^-]$. Solving eq 13 in terms of $[H^+]$ at all of the residence times provides k_3 in eq 14,

$$\frac{-d[OCN^-]}{dt} = k_1[OCN^-] + k_2[OCN^-][NH_3] + k_3K_{OCN}[OCN^-]/[OH^-] \quad (14)$$

since k_1 and k_2 are available from the rate at higher pH. The values of k_3 are given in Table 2 and reflect the rate of hydrolysis

TABLE 2: Rate Constants for Schemes 1−3 at 275 bar

temp, °C	10^3k_1, s^{-1}	10^2k_2, kg mol^{-1} s^{-1}	10^2k_3, s^{-1}	10^3k_4, s^{-1}	10^4k_5, s^{-1}	$10^{-4}k_6$, kg mol^{-1} s^{-1}
110	0.6 ± 0.2		9.4 ± 2.4			
120	1.1 ± 0.1	4.0 ± 0.7	10.6 ± 3.1			
130	2.3 ± 0.2	3.2 ± 0.7	13.3 ± 4.9			
140	3.9 ± 0.3	13.3 ± 8.7	27.9 ± 14.4	2.2 ± 0.3		
150	7.64 ± 1.1	9.6 ± 10.1	23.5 ± 1.5	4.9 ± 0.5		
160	11.7 ± 1.9	29.8 ± 8.5		9.8 ± 1.1		
170				19 ± 4		
190						6.2
200						8.5 ± 0 0.2
210					3.3 ± 1.8	11 ± 1
220					5.6 ± 3.5	14 ± 2
230					10 ± 7	17 ± 3
240					14 ± 9	17 ± 0.1
250						22 ± 9
260						40 ± 26

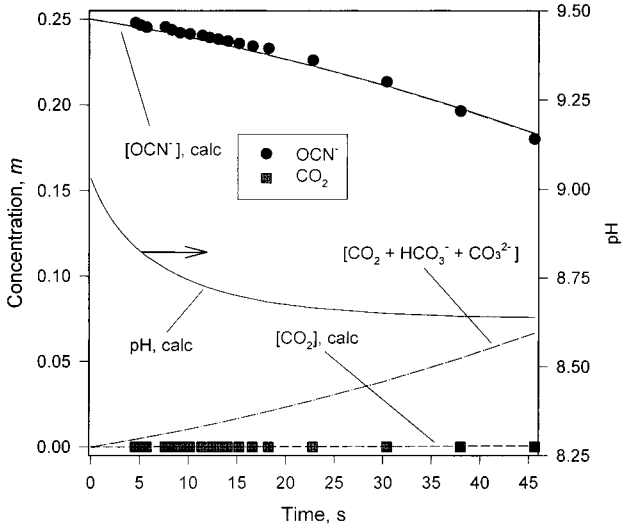

Figure 2. Calculated species concentrations and pH compared to the experimentally determined data (points) for 0.25 *m* NaOCN at 140 °C and 275 bar.

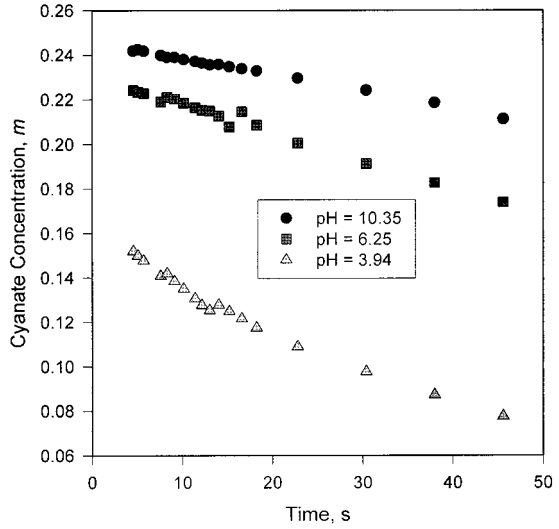

Figure 3. Time dependence of the OCN^- concentration in 0.25 *m* NaOCN at 130 °C and 275 bar as a function of the initial pH.

of HNCO, which is the dominant process at lower pH values. Note that $k_3 > k_2 > k_1$, which is consistent with previous work[9,11,12] showing that OCN^- decomposes more quickly in acidic solution than in basic solution. In fact, bubbles of CO_2 immediately formed at room temperature as the solution at pH = 3.94 was being made. Consequently, no kinetics measurements were made at this pH, but Figure 3 shows that the initial reaction rate is faster. The reason is that k_3 increasingly dominates the rate because [HNCO] is larger. $[HNCO]/[OCN^-] \approx 9$ at 150 °C.

When consistent values of k_1, k_2, and k_3 are determined over a range of pH values, the hydrothermolysis kinetics of the cyanate species can then be used as a function of pH in more complex reaction networks. Specific examples are the hydrothermolysis of the semicarbazide (SCA^+) and aminoguanidinium (AG^+) cations as nitrate salts, which are discussed next.

Kinetics of SCA^+. Semicarbazide is a weak base[26] and protonates (SCA^+) in an acidic solution. Aqueous HNO_3 was used in this work, and the resulting salt is referred to as SCAN. SCA^+ decomposes in H_2O according to reaction 15:[27,28]

$$SCA^+ + H_2O \rightarrow CO_2 + NH_4^+ + N_2H_4 \qquad (15)$$

Although N_2H_4 is a weaker base than NH_3, some $N_2H_5^+$ forms in addition to NH_4^+. The kinetics of reaction 15 were previously reported at 80 [29] and 100 °C,[30] and the rate was found to increase with increasing acidity.

We characterized reaction 15 with 0.25 *m* SCAN under hydrothermal conditions ($T = 140-170$ °C, $P = 275$ bar) using initial pH values at 25 °C of 2.1 and 5.7. The natural pH value of aqueous SCAN is 2.1, and 93% of the SCA is protonated. NaOH was added to obtain pH = 5.7. Selected IR spectra for aqueous SCAN at several residence times are shown in Figure 4 and reveal that CO_2 and the carbonyl stretch of SCA^+ can be followed. The CO_2 concentration data were weighted more heavily than the SCA^+ data because fitting of the carbonyl mode is complicated by partial interference from the bending mode of H_2O. Scheme 2 gives the reaction network employed in modeling the hydrothermolysis kinetics of SCA^+. Scheme 2 rests on the optimization of a fourth rate constant k_4 and incorporates the OCN^- kinetics of Scheme 1. The solution of Scheme 2 requires that the pH be specified at all times and can be accomplished by use of the charge balance equation

$$[H^+] + [SCA^+] + [N_2H_5^+] + [NH_4^+] + [Na^+] = [OH^-] + [HCO_3^-] + [NO_3^-] + [OCN^-] \qquad (16)$$

in its fully parametrized form as

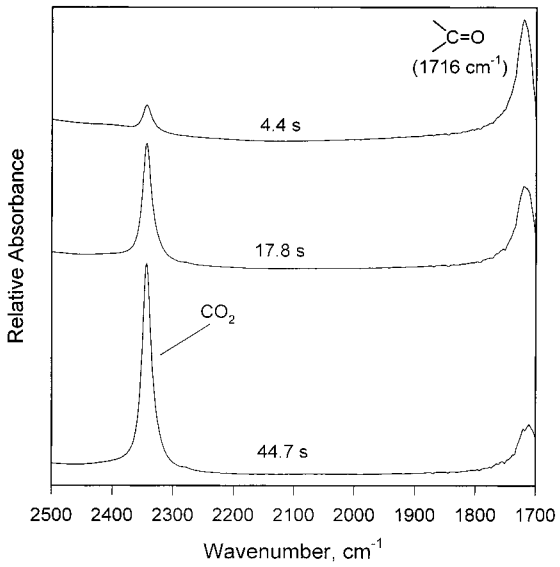

Figure 4. IR spectra at several residence times for 0.25 *m* semicarbazide (SCA^+) nitrate at 160 °C and 275 bar. The CO_2 mode area and carbonyl stretching mode area of SCA^+ (1716 cm^{-1}) have reverse trends.

SCHEME 2

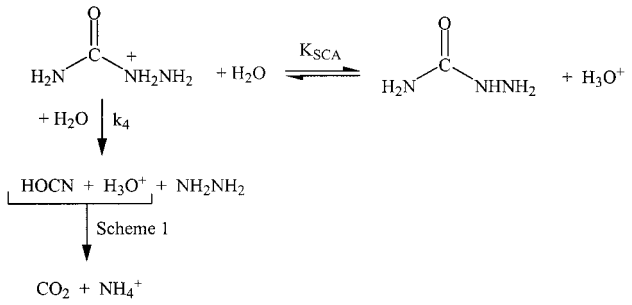

$$[H^+] + \frac{[SCA_T]K_{SCA}[H^+]}{K_W + K_{SCA}[H^+]} + \frac{[N_2H_{4T}]K_{N_2H_4}[H^+]}{K_W + K_{N_2H_4}[H^+]} + \frac{[N_T]K_N[H^+]}{K_W + K_N[H^+]} + \frac{[Na_T^+]K_{Na^+}[H^+]}{K_W + K_{Na^+}[H^+]} = \frac{K_W}{[H^+]} + \frac{[CO_{2T}]K_1}{K_1 + [H^+]} + \frac{[HNO_{3T}]K_{HNO_3}}{K_{HNO_3} + [H^+]} + \frac{[OCN_T^-]K_{OCN^-}}{K_{OCN^-} + [H^+]} \quad (17)$$

$[N_2H_{4T}] = [N_2H_4] + [N_2H_5^+]$, and $[SCA_T] = [SCA^+] + [SCA]$. $[Na_T^+]$ was included only when NaOH had been added. Figure 5 shows that the pH rises slightly during the reaction primarily because NH_3 is a product. The resulting value of k_4 is comparable in magnitude to k_3 (Table 2), which might be assumed to indicate that merely k_3 controls the overall rate of hydrothermolysis. This is not the case, however, because the carbonyl stretch of SCA^+ can also be followed as one indication. It reveals that SCA^+ disappears at a rate comparable to the rate of CO_2 formation. Thus, the similiarity of the values of k_3 and k_4 is fortuitous.

The $[NH_4]NO_3$ product is inert at the temperature and time scale of these IR spectroscopy measurements.[4] The fate of N_2H_4 is of interest. N_2H_4 is known to decompose in water at 400 °C and 350 atm in a 316 SS cell to produce NH_3, N_2, and H_2.[31] There is no evidence of further reaction of N_2H_4 or $[N_2H_5]NO_3$ in the Ti cell on the basis of the fact that the latter compound is expected to liberate N_2O,[32] which is easily detected.[14] On the other hand, when the same experiment was performed in a cell constructed of 316 SS, the prominent absorption of N_2O grows with time. After complete reaction the N_2O concentration is about 25% that of the initial SCAN concentration. Reaction 18 has been given before[32] for the thermal decomposition of $[N_2H_5]NO_3$. Since one molecule of N_2H_4 is formed by each SCA^+ decomposed, it is noteworthy that the $N_2O/([N_2H_5]NO_3)$ concentration ratio is $^1/_4$ at the hydrothermal conditions. The fact that N_2O appears in the 316 SS cell and not in the Ti cell is an indication that the reaction

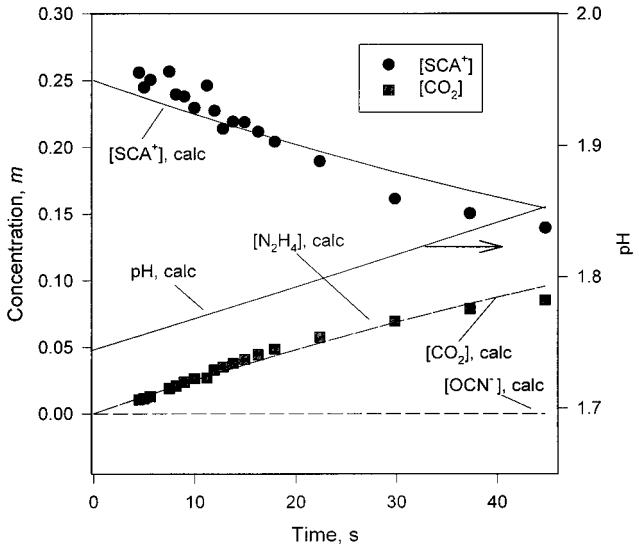

Figure 5. Calculated species concentrations and pH compared to the experimental data points in 0.25 *m* semicarbazide nitrate at 160 °C and 275 bar.

$$[N_2H_5]NO_3 \rightarrow 0.75NH_4NO_3 + 0.25N_2O + 0.33N_2 + 0.33NH_3 + 0.5H_2O \quad (18)$$

can be catalyzed by certain heterogeneous surfaces under hydrothermal conditions.

Kinetics of AG^+. Aminoguanidine is a stronger base than SCA[25,29] and is 99% protonated in H_2O at 25 °C. The natural pH of aqueous AGN is 5.6. AG^+ has long been known to hydrolyze in two steps to NH_3 and CO_2, which are summarized by the reaction

$$AG^+ + H_2O \rightarrow SCA^+ + NH_3 \quad (19)$$

followed by reaction 15.[27,33] Very limited conversion data for reaction 19 have been determined at 100 °C in acidic and basic solution.[30] The temperature range used in the work here was 190−260 °C at 275 bar, and the initial pH values (at 25 °C) were 1.6, 2.4, and 5.6. The acidic solutions were produced by adding HNO_3.

Figure 6 shows selected IR spectra of AGN at 210 °C as a function of the residence time. The absorptions of CO_2 and OCN^- are apparent, but a third absorption is observed, which was seen before in aqueous guanidinium nitrate under hydrothermal conditions.[4] This mode was hypothesized to be an overtone and/or a combination band of NO_3^- that becomes more active as a result of association of NO_3^- with the guanidinium ion at relatively high temperatures. Ion associations are favored at higher temperatures because the decreasing dielectric constant of H_2O[34] favors support of contact ion pairs over solvent-isolated ions. The origin of the 2400 cm^{-1} band is not definitely known, but its intensity decreases as the reaction progresses. As a result

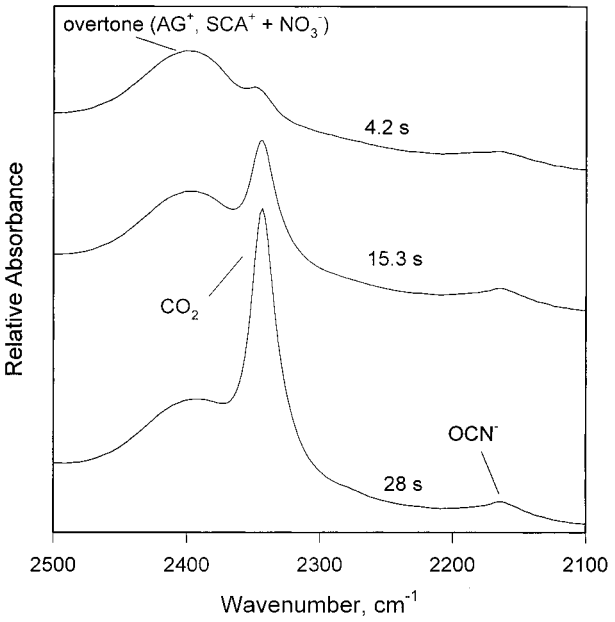

Figure 6. IR spectra of 1.00 *m* aminoguanidinium nitrate at 210 °C and 275 bar at several residence times. The OCN^- intermediate and CO_2 products are observed. The mode at 2400 cm^{-1} is possibly an overtone or combination band of NO_3^- that is activated by ion pairing with AG^+ and SCA^+.

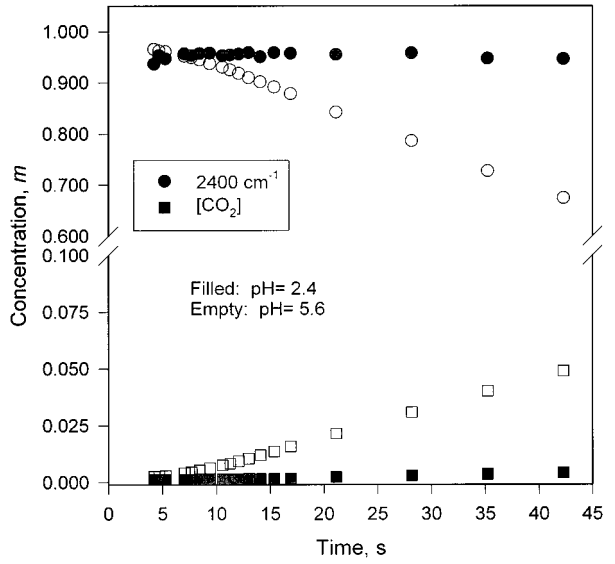

Figure 7. Comparison of the reaction rate of AGN at 210 °C and 275 bar at two values of the pH.

of the uncertainty, the kinetics analysis was based primarily on the area of the CO_2 absorption, although the OCN^- mode was also checked when fitting the overall rate. As shown by Figure 7, the rate of conversion at lower pH values is slower than at higher pH. This is opposite the trend found for SCA^+ and is consistent with earlier findings.[30]

The reaction network used to model the kinetics herein is given by Scheme 3, which incorporates Schemes 1 and 2. Scheme 3 was devised from the fact that a single rate constant k_5 at low pH could not capture the faster reaction rate at higher pH. $[OH^-]$ is larger at the higher pH values, and OH^- can act as a nucleophile to convert AG^+ to SCA with a rate constant k_6. Since SCA equilibrates with SCA^+, this pathway supplies a second route to increase the SCA^+ concentration. As before, the determination of the rate constants required the use of a time-dependent pH value during the reaction. This was accomplished with the charge balance equation

$$[H^+] + [AG^+] + [SCA^+] + [N_2H_5^+] + [NH_4^+] = [OH^-] + [HCO_3^-] + [NO_3^-] + [OCN^-] \quad (20)$$

in the parametrized form of

$$[H^+] + \frac{[AG_T]K_{AG}[H^+]}{K_W + K_{AG}[H^+]} + \frac{[SCA_T]K_{SCA}[H^+]}{K_W + K_{SCA}[H^+]} + \frac{[N_2H_{4T}]K_{N_2H_4}[H^+]}{K_W + K_{N_2H_4}[H^+]} + \frac{[N_T]K_N[H^+]}{K_W + K_N[H^+]} = \frac{K_W}{[H^+]} + \frac{[CO_{2T}]K_1}{K_1 + [H^+]} + \frac{[HNO_{3T}]K_{HNO_3}}{K_{HNO_3} + [H^+]} + \frac{[OCN_T^-]K_{OCN^-}}{K_{OCN^-} + [H^+]} \quad (21)$$

$[AG_T] = [AG^+] + [AG]$. By use of the complete rate expression for Scheme 3, which incorporates Schemes 1 and 2, the rate constants k_5 and k_6 can be optimized and are given in Table 2. Figure 8 shows the concentration−time profiles obtained for AG^+ at 230 °C. The pH initially drops sharply because H^+ is released in the formation of a weak base (SCA) from a stronger base (AG). As the SCA reacts and NH_3 and CO_2 are formed, the H^+ solution rapidly becomes buffered and the pH stabilizes at a relatively constant value. In the pH range used, $k_6 \gg k_5$, but since $[OH^-]$ is relatively low, the effect of k_6 on the overall rate of AG^+ conversion is modest. The 2400 cm^{-1} mode was arbitrarily fit for illustration purposes as being the result of a 75% contribution of AGN and a 25% contribution of SCAN. This mode was not used in the refinement of the kinetic model. As before, $[N_2H_5]NO_3$ remained unreacted in the Ti cell, as indicated by the absence of an IR absorption for N_2O.

Arrhenius Parameters. These studies are the first measurements of the reaction rates in Schemes 1−3 in the hydrothermal regime. It is useful to compare them with several rates given previously for the normal liquid range of H_2O. This comparison is easily made with the Arrhenius plot shown in Figure 9 for k_1−k_6. The pH values used previously are sometimes outside the range used here, which complicates direct comparisons. Table 3 gives the Arrhenius parameters for the hydrothermal regime from the present work.

The hydrothermolysis rate of NaOCN in H_2O (k_1) predicts a lower rate than was found at 22 °C [2] and a higher rate than was found for pH = 13 at 70−94 °C.[11] Because the rate of this reaction decreases with increasing pH, the data are more consistent with the higher pH data of Jensen.[11] The autocatalytic rate constant k_2 extrapolates well to values reported previously at 18−50 °C.[12] However, the catalyst proposed in our work is NH_3 rather than HCO_3^-, which was proposed earlier. Hydrolysis rate of HNCO in acid solution, k_3, extrapolates reasonably well to the rates reported earlier at 4 and 10 °C,[11] although the rate at 4 °C is very tenuous. The acid and neutral hydrothermolysis rate constant for SCA^+, k_4, predicts a faster rate than previous data at 80 [29] and 100 °C suggest,[30] whether extrapolated from lower to higher temperature or higher to lower temperature. The rate constant for acid hydrothermolysis of AG^+, k_5, extrapolates well to the rate previously reported at 100 °C.[30] Because most of the rate constants for this system are consistent with past studies, we have confidence that they are valid for use in hydrothermal reaction networks at least in the pH range for which the rates were determined. They may not be valid for very highly acidic or basic solutions.

SCHEME 3

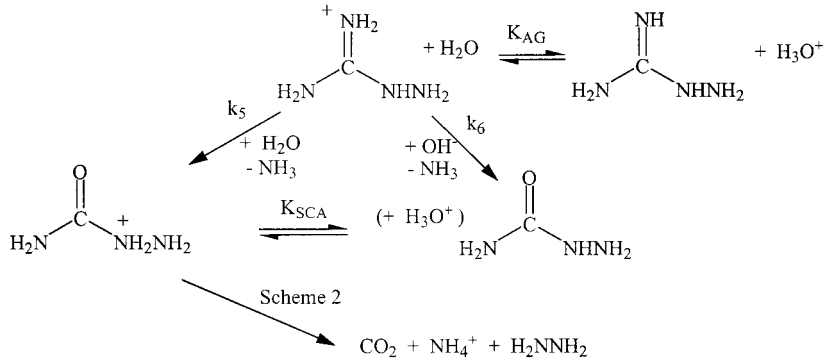

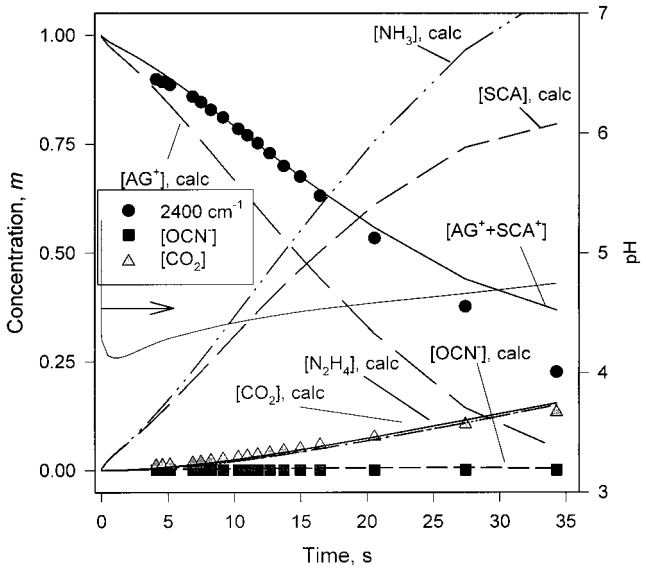

Figure 8. Calculated species concentrations and pH compared to the experimental data for 1.00 *m* AGN at 230 °C and 275 bar.

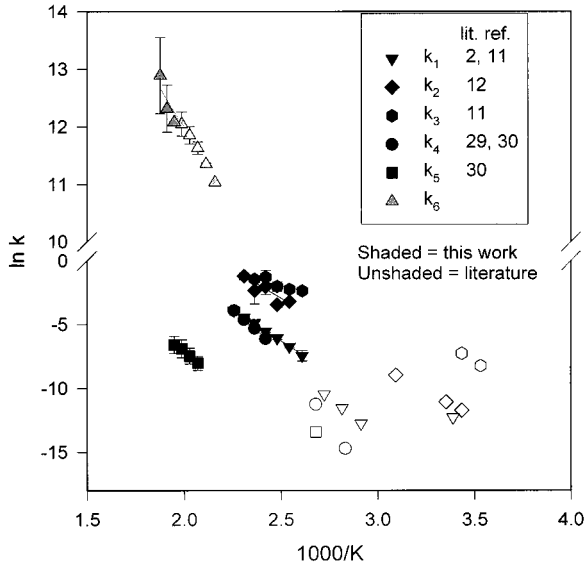

Figure 9. Arrhenius plot of the hydrothermal rate constants from this work compared to previously reported rate data at ≤100 °C for the same or similar reactions.

This study highlights the value of developing kinetics and mechanism schemes for hydrothermal reactions of complex molecules by working from the rates of the products back to the reactants. The products tend to be relatively simple families of compounds that can be expected to be common to many types of reactants. The reactants can be relatively more complex molecules that eventually hydrothermalize to these simpler families of intermediates and products. Although the number of reactions is still not large (6−10) in the schemes studied here and elsewhere,[5,13] it has been possible to specify the rates of multistep pathways in considerable detail and to develop a consistent set of individual rate constants.

TABLE 3: Arrhenius Parameters for the Rate Constants in Schemes 1−3

rate constant	E_a, kJ/mol	ln(A, s^{-1})
k_1	80.7 ± 1.8	18.1 ± 0.5
k_2	74.7 ± 9.6	19.6 ± 2.7[a]
k_3	30.3 ± 8.5	7.2 ± 2.4
k_4	109.2 ± 2.0	25.8 ± 0.5
k_5	90.7 ± 10.7	14.8 ± 2.6
k_6	47.0 ± 4.3	23.3 ± 1.0[a]

[a] In units of kg mol^{-1} s^{-1}.

Acknowledgment. We are grateful to the Army Research Office for support of this work on DAAG55-98-1-0253 with Dr. R. W. Shaw as the program manager. Dr. J. W. Schoppelrei performed some initial studies on AGN.

References and Notes

(1) Kieke, M. L.; Schoppelrei, J. W.; Brill, T. B. *J. Phys. Chem.* **1996**, *100*, 7455.
(2) Wen, N.; Brooker, M. H. *Can. J. Chem.* **1994**, *72*, 1099.
(3) Maiella, P. G.; Brill, T. B. *Appl. Spectrosc.* **1996**, *50*, 829.
(4) Schoppelrei, J. W.; Kieke, M. L.; Wang, X.; Klein, M. T.; Brill, T. B. *J. Phys. Chem.* **1996**, *100*, 14343.
(5) Belsky, A. J.; Brill, T. B. *J. Phys. Chem. A* **1998**, *102*, 4509.
(6) Maiella, P. G.; Brill, T. B. *J. Phys. Chem.* **1996**, *100*, 14352.
(7) Maiella, P. G.; Brill, T. B. *J. Phys. Chem. A* **1998**, *102*, 5886.
(8) Belsky, A. J.; Maiella, P. G.; Brill, T. B. *J. Phys. Chem. A* **1999**, *103*, 4253.
(9) Lister, M. W. *Can. J. Chem.* **1955**, *33*, 426.
(10) Amell, A. R. *J. Am. Chem. Soc.* **1956**, *78*, 6234.
(11) Jensen, M. B. *Acta Chem. Scand.* **1958**, *12*, 1657.
(12) Jensen, M. B. *Acta Chem. Scand.* **1959**, *13*, 659.
(13) Belsky, A. J.; Brill, T. B. *J. Phys. Chem. A* **1999**, *103*, 3006.
(14) Maiella, P. G.; Schoppelrei, J. W.; Brill, T. B. *Appl. Spectrosc.* **1999**, *53*, 351.
(15) Cvetanovic, R. J.; Singleton, D. L. *Int. J. Chem. Kinet.* **1977**, *9*, 81.
(16) Cvetanovic, R. J.; Singleton, D. L. *Int. J. Chem. Kinet.* **1977**, *9*, 1007.
(17) Kortum, G.; Vogel, W.; Andrussow, K. *Dissociation Constants of Organic Acids in Aqueous Solutions*; Butterworths: London, 1961.
(18) *Ammonia*; Subcommittee on Ammonia, University Press: Baltimore, MD, 1979.
(19) *Ionization Constants of Inorganic Acids and Bases in Aqueous Solutions*, 2nd ed.; Perrin, D. D., Ed.; Pergammon Press: New York, 1982.
(20) Lindsay, W. T. *Proc.—Int. Water Conf., Eng. Soc. W. Pa.* **1980**, *41*, 284.
(21) Marshall, W. L.; Franck, E. U. *J. Phys. Chem. Ref. Data* **1981**, *10*, 295.

(22) Werner, E. A.; Fearon, W. R. *J. Chem. Soc.* **1920**, *117*, 1256.
(23) Fearon, W. R.; Dockeray, G. C. *Biochem. J.* **1926**, *20*, 13.
(24) Kemp, I. A.; Kohnstam, G. *J. Chem. Soc.* **1956**, 900.
(25) Maiella, P. G.; Brill, T. B. *Inorg. Chem.* **1998**, *37*, 454.
(26) Lieber, E.; Smith, G. B. L. *Chem. Rev.* **1939**, *25*, 213.
(27) Thiele, J. *Ann.* **1892**, *270*, 35.
(28) Maselli, G. *Gazz. Chim. Ital.* **1905**, *35*, 267.
(29) Travagli, G. *Gazz. Chim. Ital.* **1958**, *88*, 1135.
(30) Lieber, E.; Smith, G. B. L. *J. Am. Chem. Soc.* **1937**, *59*, 2283.
(31) Rubtsov, Yu. I.; Manelis, G. G. *Russ. J. Phys. Chem.* **1970**, *44*, 220.
(32) Masten, D. A.; Foy, B. R.; Harridine, D. M.; Dyer, R. B. *J. Phys. Chem.* **1993**, *97*, 8557.
(33) Ponzio, G.; Gastaldi, G. *Gazz. Chim. Ital.* **1913**, *43*, 129.
(34) Uematsu, M.; Franck, E. U. *J. Phys. Chem. Ref. Data* **1980**, *84*, 758.